

Residual strength analysis of AA2198 laser beam welded integral structures

Alexandre Amorim Carvalho
aac@ist.utl.pt

Instituto Superior Técnico, Lisboa, Portugal

October 2014

Abstract

To meet the future demands of the aerospace industry with respect to safety, productivity, weight and cost, new materials and joining concepts have been developed. Recent developments in the metallurgical field now make it possible to use laser-weldable Aluminum Alloys (AA) of the 2xxx series, such as the AA2198, with a high structural efficiency index due to their high strength and low density. The European structural integrity assessment procedure (SINTAP) combined with FEM approach was used for the assessment of the fracture mechanical behavior of the laser beam-welded integral structures. An experimental program which included tensile, CTOD and residual strength tests was performed to mechanically characterize the AA2198 in the T3 and T8 tempers. Structures were numerically modeled using shell elements and the stress intensity factors were extracted using energy methods such as the J-integral and Virtual Crack Closure Technique (VCCT). Residual strength predictions were successfully made proving the reliability of the SINTAP procedure. The damage tolerance behavior of the AA2198 integral structures was compared with the AA6013 integral structures and revealed the promising capabilities of the AA2198.

Keywords: Laser beam welding, aluminum lithium, SINTAP, stiffened panels, damage tolerance, FEM

1. Introduction

A new generation of Aluminum-Lithium (Al-Li) alloys with a higher toughness and better resistance to corrosion is being developed by the main Aluminum Alloys (AA) producers to fulfill the requirements of aircraft structural components. The objective is to counteract the growth of composites usage in fuselages and structural components of airplanes [1].

Laser beam welding (LBW) is already used in the aeronautical industry and fuselages from the AA6xxx series are already existing namely in the lower fuselage panels because the welded panels provide higher buckling strength and lower weight compared with classical riveted designs [1]. The absence of material required for the overlapping in this LBW joining technology makes it highly suitable for aircraft designs.

LBW structures require changing from the concept of differential riveted structures to integral structures which introduces a different structural behavior and fracture mechanisms. As far as the author knows, studies investigating the damage tolerance of welded integral structures of Al-Li alloys are scarce however. The main emphasis of the current study is to investigate the mechanical fracture

behavior of AA2198 base material panels and laser beam welded integral structures.

The study performed in this thesis is part of a thematic called "Extrapolation and technical and economic study of a laser beam welding technology" which is under financial support of the European Union Clean Sky EU - JTI Platform.

2. Background

2.1. Residual Strength

For Linear Elastic Fracture Mechanics (LEFM), which is based on elasticity, the effects of more than one type of loading on the crack tip can be determined by linearly adding the stress intensity factor (SIF). In the case of riveted stiffened panels with crack between stiffeners, the SIF and consequently the crack growth and the residual strength is influenced by the crack growth in the unstiffened panel and by the effect of the stringers riveted onto the skin.

A fuselage structure, which is stiffened by stringers riveted to the skin, may contain a skin crack and may fail due to either of the following criteria [2]:

- Failure of the skin due to instability of the crack;

- Failure of the stiffener perpendicular to the crack;
- Failure of the fasteners attaching the stiffeners perpendicular to the crack.

Assuming that the fasteners are rigid, the displacement of adjacent point of skin and stringer are equal. The developing crack in the skin causes a larger displacement in the skin which will be transmitted to the stringer. This means that the stringer takes load from the skin and, consequently, the displacements in the cracked skin are smaller than in an unstiffened panel leading to lower skin stress and lower stress intensity factor [3].

Built-up structure and integral structure may develop different damage scenarios which will represent different damage study approaches. Integral welded structures are already used for fuselage panels of specific single aisle and wide body aircraft types in the forward and aft bilge area [2].

2.2. Defect assessment procedures

In cases where defects (cracks, fabrication flaws, in-service flaws) are (or could be) present in safety-critical welded structures such as pressure vessels, it is both prudent and efficient to develop standardized methods to evaluate them. These methods, known as Fitness For Purpose (FFP), Fitness For Service (FFS) or Engineering Critical Assessment (ECA), can be used for various applications such as demonstrating a safety case, extending operational life or calculating defect acceptance criteria for welded fabrication of a new structure.

Since the R6 was released in 1976 [4], many more procedures were introduced in worldwide industries. Other developed procedures were the British Standard PD6493 [5] which is a guide to methods for assessing the acceptability of flaws in fusion welded structures; the Engineering Flaw Assessment Method (EFAM) [6], developed in Germany, is a comprehensive method for the flaw assessment referring to the determination of the crack resistance of materials and the crack tip loading in a cracked component and the Swedish procedure SAQ [7] for failure assessment of structures containing defects made for the nuclear power industry. Other assessment procedures were developed in France, Japan, China and the United States [8, 9, 10, 11].

In 1996 the Structural INTtegrity Assessment Procedure (SINTAP) was released. The core of the SINTAP consists of elements from the R6 method [4], the Engineering Treatment Model (ETM) [12], which was developed by the Helmholtz Zentrum Geesthacht (HZG) for internal use, and SAQ [7]. It provides an estimation of the crack tip loading in a cracked structural component which can then be compared with the material toughness value to

assess the structural integrity.

Recently, an European Thematic Network on the Fitness-for-Service (FITNET) has developed a comprehensive flaw assessment procedure by updating the SINTAP procedure and combining it with other failure modes of fatigue, creep and corrosion in one document.

3. Methodology

3.1. SINTAP procedure

The use of the SINTAP was made with the help of Python scripts that were developed to simulate the Crack Driving Force. The CDF is plotted together with the respective material R-curve. At each intersection point between the CDF and R-curve it is possible to find the respective applied load together with the stable crack extension and the corresponding crack tip loading. The structural response can then be predicted by plotting the load versus stable crack extension or load versus CTOD. This is represented in figure 1

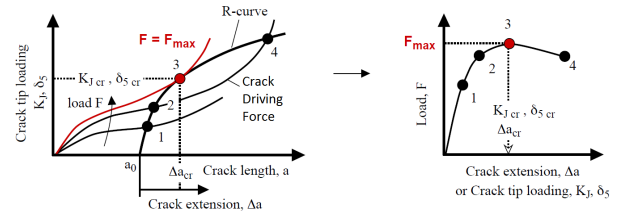


Figure 1: Principle of the residual strength analysis [13]

Plasticity effects due to primary stresses are evaluated automatically by means of the expression $f(L_r)$ where $L_r = F/F_Y$. Because the SINTAP introduces its own plasticity correction, there is no need to consider it for the R-curve and FEA. In this work, two levels of analysis will be presented. The Level 1 and Level 3 of analysis will be applied to a M(T) specimen and to an equal M(T) specimen with four laser beam welded stringers which will be referenced as four-stringer panel.

3.1.1 Level 1

The level 1 of analysis requires the Young's modulus, E , the proof strength, $R_{p0.2}$, and the tensile strength, R_m . The plasticity correction function of the Level 1 is defined as:

$$f(L_r) = \begin{cases} (1 + 0.5L_r^2)^{-1/2} [0.3 + 0.7\exp(-\mu L_r^6)] & \text{for } L_r \leq 1, \\ f(1) L_r^{(N-1)/2N} & \text{for } 1 < L_r \leq L_r^{max}, \\ 0 & \text{for } L_r > L_r^{max} \end{cases} \quad (1)$$

where N , the strain hardening exponent, and μ is:

$$N = 0.3 \left[1 - \frac{R_{p0.2}}{R_m} \right], \quad \mu = \min \left[0.6, 0.001 \frac{E}{R_{p0.2}} \right] \quad (2)$$

The equation presented here is referring to the case of materials with continuous stress strain curves.

3.1.2 Level 3

The plasticity correction function $f(L_r)$ of the Level 3 is defined as:

$$\begin{cases} [E\epsilon_r/\sigma_r + 0.5L_r^2/(E\epsilon_r/\sigma_r)]^{-1/2} & \text{for } L_r \leq L_r^{max}, \\ 0 & \text{for } L_r > L_r^{max}, \end{cases} \quad (3)$$

where ϵ_r is the material's true strain obtained from the uniaxial stress strain curve at a true stress σ_r of the equivalent engineering stress $\sigma = L_r R_{p0.2}$.

3.2. Experimental

3.2.1 Tensile tests

These were performed in an electromechanical 100kN SCHENCK TREBEL universal testing machine according to DIN EN 6892 with a displacement control speed of 0.5 mm/min and measurements of the applied displacement and the applied force were taken directly from the machine instruments to a support computer. The software used to collect the data was TestExpert 11.0.

3.2.2 CTOD tests

Compact tension C(T) specimens with different thicknesses were used (3.2mm and 5.0mm). The tests consisted of three steps: Pre-fatiguing, crack propagation and re-fatiguing; all according to the EFAM GTP 02 [14].

All specimens were subjected to pre-fatiguing using a Schenck 10kN servohydraulic machine for 10000 - 20000 cycles with a frequency of 20Hz. The same machine was used for the CTOD testing and, during this test, the specimens were submitted to an increasing displacement of 0.25 mm/min.

To make the CTOD readings and data treatment a HBM (Hottinger Baldwin Messtech) MGC+ data acquisition machine was used. This machine makes the interface between the sensors and the computer that was used to record the data from the tests: CTOD δ_5 , applied force, CMOD. The setup consisted of two CTOD clips and one CMOD clip. This can be seen in figure 2

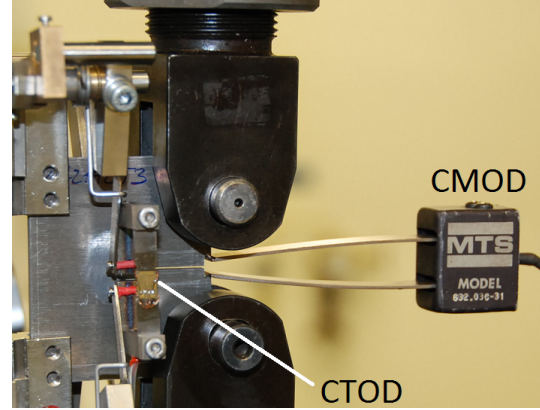


Figure 2: CTOD test setup

For the construction of the R-curves, the multiple specimen method was used to measure stable crack growth. For each CTOD test a δ_5 was chosen. When the CTOD would reach the desired value, the test was stopped and an unloading with displacement control of -0.25 mm/min was imposed.

One point per test was used to build the R-curves. According to the norm used, the measured $\delta_5 - \Delta a$ curve is fitted by a power law equation and must have the form:

$$\delta_5 = A + C(\Delta a)^D \quad (4)$$

where A and C are higher or equal to zero and D has a value between zero and one, both inclusive.

3.2.3 Residual strength test

Residual strength tests were planned using panels with two different configurations. A schematic of both panels can be seen in figure 3. For each specimen one experiment was made and the Potential Drop method [15] was used.

The skin of the panels used in these tests was a 5.0mm thick rolled plate made of AA2198 in the T3 thermal condition. The stringers were of a 3.2mm thick rolled plate in the T8 condition and also 1.9mm thick milled from the same 3.2mm thick rolled plate as seen in figure 4.

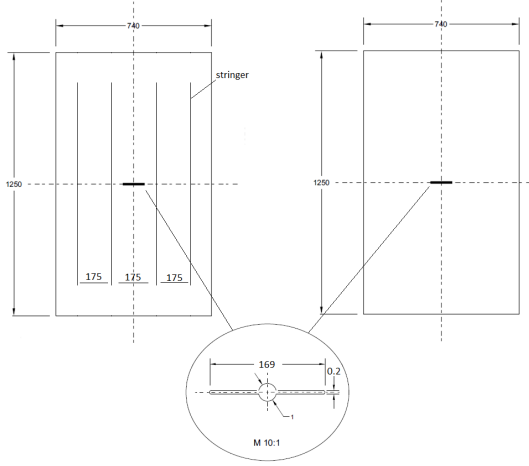


Figure 3: M(T) specimen and four-stringer panel

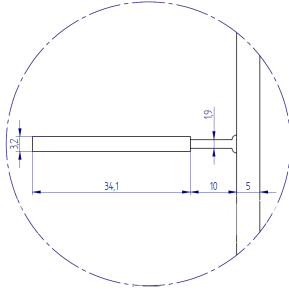


Figure 4: Detail of the stringer dimensions.

An anti-buckling guide was used to prevent out-of-plane bending. Buckling can occur due to a local compression stress induced by the crack. In this case of uniaxial tensile applied load, a second principal stress component is negative around the crack. This effect is well described in [16, 17].

A servohydraulic machine (Schenck hydraulic universal testing machine) with 2500 kN capacity was used for these tests at room temperature. During the experiment the quasi-static displacement controlled loading rate was 1.0mm/min.

During the residual strength tests, the following parameters were recorded: applied load, CMOD, CTOD δ_5 and the total elongation (ν_{LL}) starting at a gauge length L_0 .

With these instruments plus the input values for the machine, the parameters recorded on graphs were: δ_5 at the left and right side, CMOD, the displacement ν_{LL} , the applied load and the electric potential. The crack length value at each moment can then be obtained directly from the Johnson formula [18, 15]. But the Johnson formula can only be used for the M(T) specimen because the four-stringer panel evaluation would require consideration for the weld conduction properties which wasn't available.

Before the test took place, the specimens were submitted to a cyclic loading until a fatigue crack

length of approximately 2mm was achieved to obtain a sharp starting crack. After the test, the panels were submitted to re-fatiguing in order to open them without damaging the crack surface.

3.3. Numerical

In order to apply the SINTAP procedure to stiffened panels, it is required to predict the SIF distribution for different crack sizes. These solutions are based on FEM results. The methods and models used were firstly verified for the case of the unstiffened M(T) specimen where there are published analytical solutions for the SIF distribution [19].

Python scripts, together with Patran (used as pre-processor) and Abaqus (processor), were effective to generate the required data. Three methods were tested to obtain the SIF distribution: Compliance, J-integral and Virtual Crack Closure Technique (VCCT).

Another input required for the SINTAP applied to the four-stringer panel is the load increase in the stringer element for a growing crack size. This load increase can be expressed by a load concentration factor L_s :

$$L_s \left(\frac{a}{W} \right) = \frac{F_{str}}{F_{str}^*} \quad (5)$$

which is defined by the ratio of the stringer load in the cracked structure, F_{str} , and the stringer load in the intact structure, F_{str}^* .

Unstiffened and stiffened panels were modeled with shell elements which are widely used for thin-walled structures in the aerospace industry. The quadrilateral linear shell element S4 (ABAQUS) was chosen for both the skin and stringers of the panels.

Due to the presence of double symmetry, a quarter of the entire model is sufficient as demonstrated in figure 5. The quarter model has zero displacement boundary conditions on the left and the lower walls with $u_x = 0$ and $u_y = 0$, respectively.

In order to ease the change of parameters in the simulation, a model was generated where one guiding node was placed 200mm above the left wall and a connection - Kinematic Coupling option in ABAQUS - was made between this node and all the nodes on the top surface. The nodes on the surface can move on the x direction and will have the same vertical displacement as the guiding node, all other remaining DOF are fixed. The load was introduced through the skin by applying a constant displacement to the guiding node.

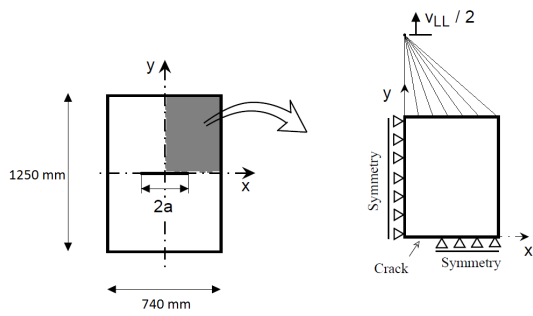


Figure 5: One quarter of model representation

The four stringer FE model contained one extra boundary condition in order to introduce the anti-buckling guide effect. A condition of zero displacement in the z direction was introduced in the lower 7.5mm of the skin. For the stringer nodes intersecting it, this condition was not applied.

The size of the smallest element was 1mm for the M(T) specimen model and 0.5mm in the four-stringer panel model.

4. Results and Discussion

4.1. Experimental

The tensile test results, presented in figure 6, provide valuable data. The AA2198 reveals an anisotropic behavior: higher strength when the load is applied in the sheet rolling direction (L) and higher plastic deformation when it is applied transversely to the rolling direction (T). The T8 temper presents approximately 45% more yield stress and 14% more ultimate tensile stress and is, therefore, a stronger condition.

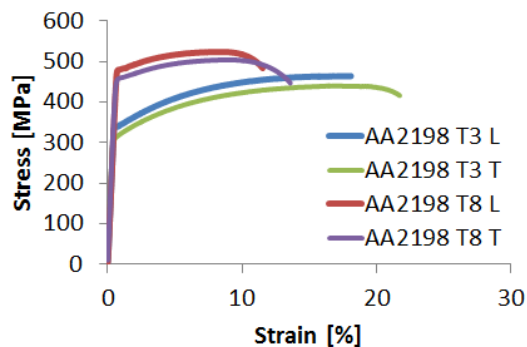


Figure 6: Stress-strain curves

CTOD tests were accomplished for four specimen types. In figure 7, the fracture resistance curves are presented where the first letter corresponds to the load application direction and the second is the crack growing direction both in relation to the sheet rolling direction (L - Longitudinal, T - Transverse). Power law equations were estimated for the extracted points.

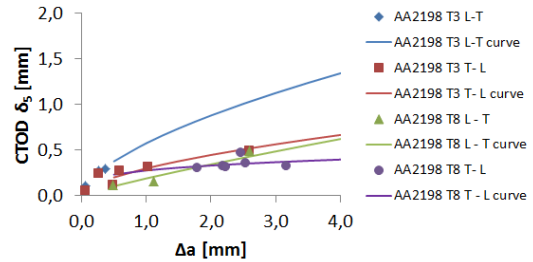


Figure 7: CTOD R-curves

Residual strength test results of the M(T) specimens were in good agreement with the C(T) specimens; the crack resistance curve observed matched with the points previously extracted.

A second residual strength test was conducted to the four-stringer panel. This test was stopped before the panel could go under unstable crack extension. Due to this premature stop the crack branching effect, which is systematically observed in integral structures, was not verified.

By the use of Scanning Electron Microscopy (SEM), the skin-stringer intersection fracture was analyzed. As can be seen in figure 8: the pre-fatigue striations are depicted in the left side of the figure and the stable crack extension is visible in the lower center-right side where the presence of dimples creates a rough surface. The Heat Affected Zone (HAZ) corresponds to the smooth surface on the top center-left of the figure which depicts the presence of a shear stress component. On the very top of the figure, a secondary crack is visible, which is situated between the HAZ and the Fusion Zone (FZ).



Figure 8: SEM: Crack extension and skin-stringer intersection

Figure 9 shows the FZ and the HAZ. It is possible to observe that the FZ has large pores, as can be expected from the welding of AA2198 [20], but these are not the main cause of the fracture. The slopes between the HAZ and the FZ are the melt

lines and are depicted by secondary cracks which occurred during the test. In this boundary there is a stress concentration due to the hardness loss and weak texture of the materials, which was already demonstrated in [1]. These observations lead to the conclusion that a sudden crack growth jump across the weld occurred while crack branching could not be verified.

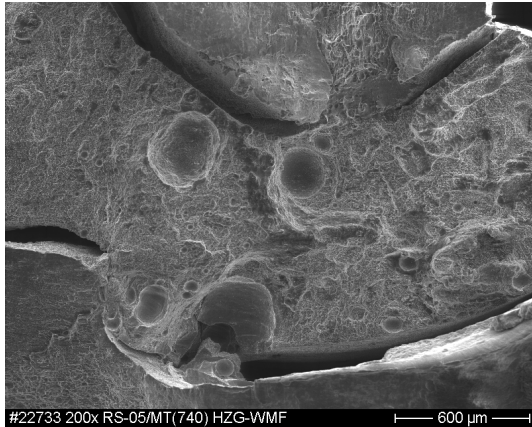


Figure 9: SEM: HAZ and FZ of the fracture surface of the four-stringer panel in the skin-stringer intersection

Comparing the data obtained from the two panels submitted to the residual strength test, it is possible to see in figure 10 that the four-stringer panel resists 20% more load and presents higher stiffness than the M(T) specimen. The higher stiffness is justified by the fact that the initial crack was placed just before the stringer.

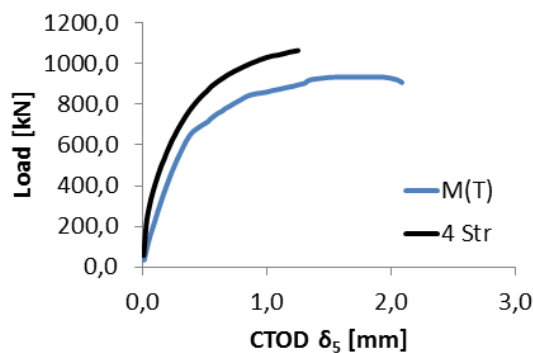


Figure 10: Residual strength tests: Load vs. CTOD curve. M(T) specimen vs. four-stringer panel.

Figure 11 depicts the higher elastic modulus of the four-stringer panel even though the panels reach to a similar ultimate stress.

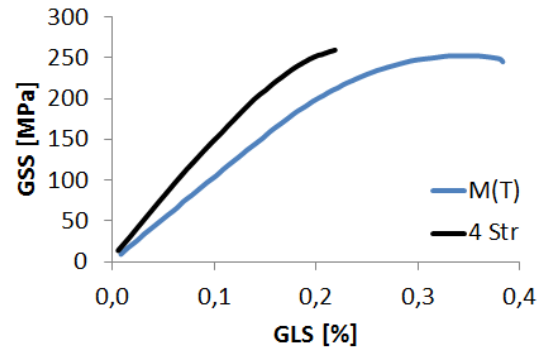


Figure 11: Residual strength tests: Gross Section Stress (GSS) vs. Gauge Length Strain (GLS)

By plotting the CTOD with the GLS, figure 12, one can see that, for the same value of strain, the four-stringer panel presents higher values of CTOD. As the skin crack tip approaches the stringer, more load is transferred into the stringer. Thus, the skin stresses in this region are reduced and, consequently, the crack tip opening must be higher and crack tip blunting occurs.

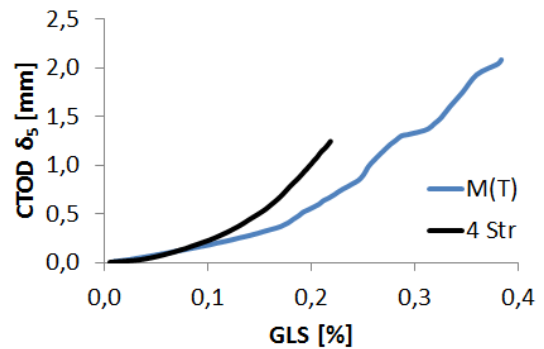


Figure 12: Residual strength tests: CTOD vs. GLS

Even though it was expected, it was not clear if crack branching occurred or not. This uncertainty would imply different SINTAP analysis: one considering crack branching occurrence and another without.

4.2. Numerical determination of SIF

Using the numerical model of the M(T) specimen, three methods for obtaining the SIF distribution were tested: Compliance, J-integral and VCCT. It can be seen in figure 13 that, while the VCCT and the J-integral methods presented accurate approximations to the analytic solution, the Compliance method revealed to be insufficient. For the SIF distributions presented, the VCCT method was used.

The normalized SIF distribution considering that crack branching occurred through the stringer is presented in figure 14 for the skin and stringer. There, it is possible to observe three singularities: at $a/W = 0.24$: the intersection between the skin

and the stringer; at $a/W = 0.26$: thickness variation of the stringer and at $a/W = 0.36$: end of the stringer interference; where a is the crack length and W is half the panel width. These singularities are common and typical of thickness variations [21].

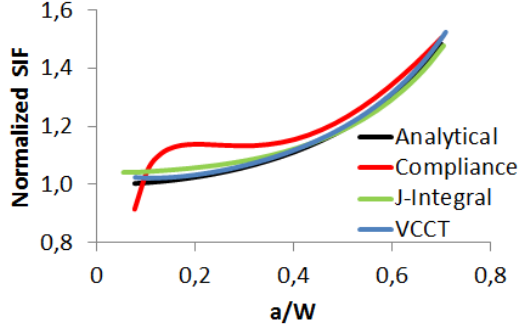


Figure 13: SIF extraction methods

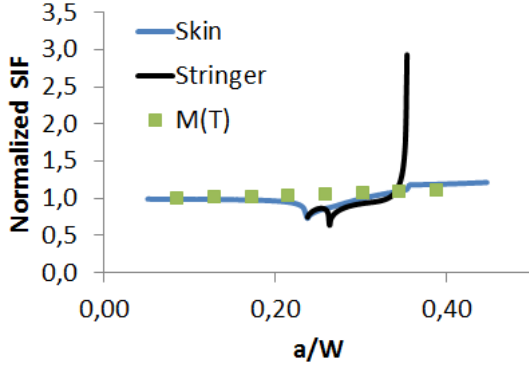


Figure 14: SIF of the four-stringer panel considering crack branching

If crack branching is not considered, then the SIF is fairly different of what is seen in figure 15. In this plot it is visible that the SIF values will sharply fall after the skin-stringer intersection. Here the skin stresses will be relaxed due to the load transition to the stringer.

In figure 16, where $*$ denotes the fact that no crack is considered and F_{str} is the load supported by the stringer, the load distribution on the stringer is plotted with the increase of the crack size for both cases in study: with and without crack branching. There it is possible to observe an increase of the ratio since the very beginning. While the crack extends through the skin, the cross sectional area of the skin supporting the load will be decreasing and forcing the stringer to support an increasing fraction of the total load. Immediately before the crack reaches the stringer there is a fast increase on the load ratio and this is visible in both curves of the plot.

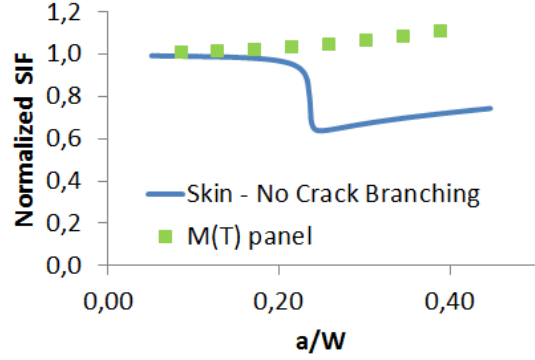


Figure 15: SIF of the four-stringer panel not considering crack branching

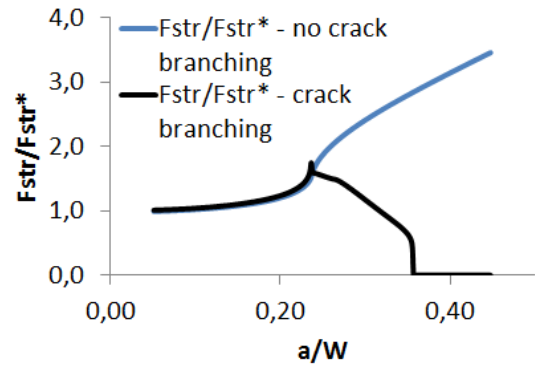


Figure 16: Load distribution on the middle stringers

In the case of the crack branching occurrence, when the crack starts propagating through the stringer, the load will be transferred to the remaining skin and outer stringer and, so, the calculated ratio will decrease. It is possible to observe in the plot that this decrease has one trend for the thinner part of the stringer (1.9mm) and another trend for the thicker part of the stringer (3.2mm).

If crack branching is not considered, the ratio will have a rapid increase after the crack passes the stringer and, shortly after this, the ratio will have a constant increase announcing a possible eminent crack branching.

4.3. Residual Strength predictions

By the use of the SINTAP procedure, the predictions of the residual strength for the M(T) specimen were performed. Figures 17 and 18 compare the Level 1 and Level 3 of analysis with the experimental curve.

By visual inspection of the presented plots, it is possible to see that the level 1 shows better approximations to the experimental curve and the level 3 over-estimates the residual strength. For the M(T) specimen case, the Level 1 would represent a better option because, not only it is an underestimation

of the maximum load, it is also a closer approximation.

Comparing the curves of the two levels, they are quite similar due to the low hardening capacity of the AA2198. This low hardening capacity is visible in the true stress strain curve of the material which does not make any improvement in the accuracy of the results for level 3.

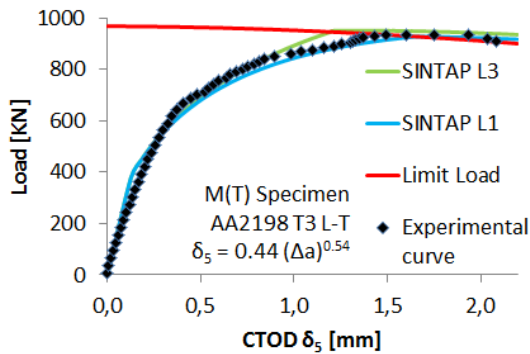


Figure 17: SINTAP analysis of M(T) specimen: Load vs. CTOD

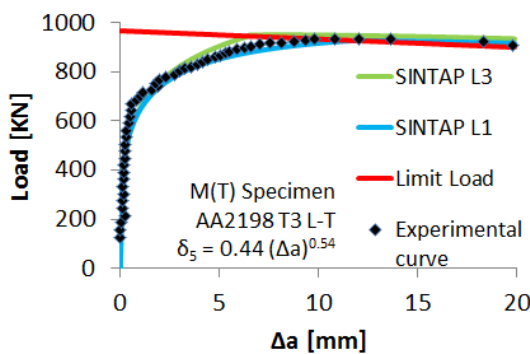


Figure 18: SINTAP analysis of M(T) specimen: Load vs. crack extension

When applying the SINTAP to the four-stringer panel, a more complex approach need to be considered. From different tested variations, there are two which deserve to be mentioned.

The first variation considers a skin failure criterion and a stringer failure criterion. In this case, the SIF distribution corresponds to the crack branching and is shown in figure 14 is applied. The skin failure criterion over-estimates the CTOD and under-estimates the maximum load while the stringer failure criterion does exactly the opposite. Following this variation, it can be observed that the experimental results are correctly between both analyzed elements which can be seen as lower and upper limits of prediction. This variation presents a consistent approximation. The best approximation is obtained by Level 3.

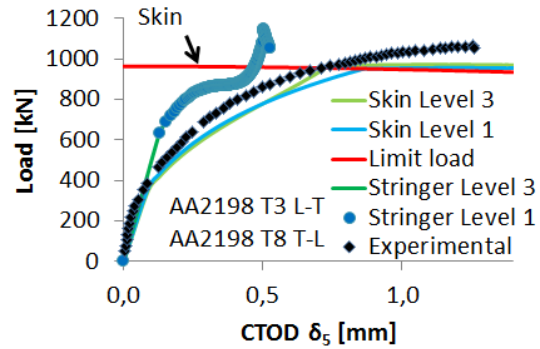


Figure 19: SINTAP analysis of the four-stringer panel, first variation: Load vs. CTOD

The second variation, presented in figure 20, considers no crack branching and only the skin failure criterion is taken to account. The FEM SIF solution for the case of no crack branching is used here. The maximum load is under-estimated and the CTOD is over-estimated but is possible to see that the load - CTOD curve has a good agreement. In this case, the Level 3 is the best approximation.

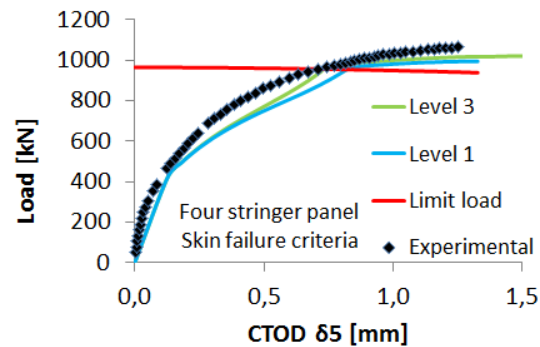


Figure 20: SINTAP analysis of the four-stringer panel, second variation: Load vs. CTOD

Assuming now another four-stringer panel made of the AA6013 T6, a comparison between the two alloys was made. When firstly analyzing the tensile behavior of the AA6013 T6 [13], the higher yield stress and lower ultimate stress in comparison with the AA2198 T3 are clear. As could be expected from the higher plastic deformation, the fracture resistance curve (CTOD - Δa) of the AA2198 T3 is better for small crack extension values but both curves tend to the same behavior when the crack extension grows to higher values.

In figure 21, the first variation (variation 3) of analysis for the four-stringer panel is plotted with the AA6013 T6 possibility against the current structure. Both AA6013 curves are between the skin and stringer failure criterions of the AA2198 which have different tempers: T3 and T8, respectively. It is possible to correlate that the yield stress takes

a very high influence on the final results having a direct relation to the maximum load.

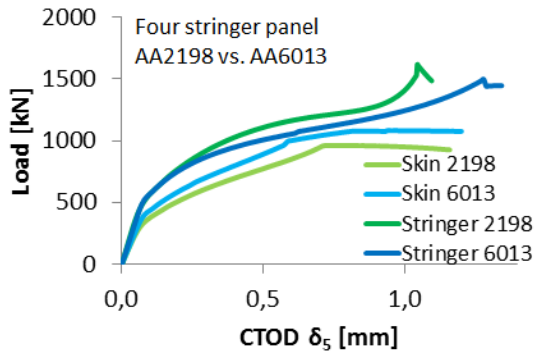


Figure 21: SINTAP analysis, variation 3: AA2198 Vs. AA6013

Considering the second variation (variation 5) of analysis in figure 22, the conclusions taken in the previous variation maintain. In fact, even though the AA2198 T3 LT CTOD curve is apparently better than the AA6013 T6 LT, the crack resistance curve has a minor contribution to the structural behavior when compared to the elastic properties of the materials.

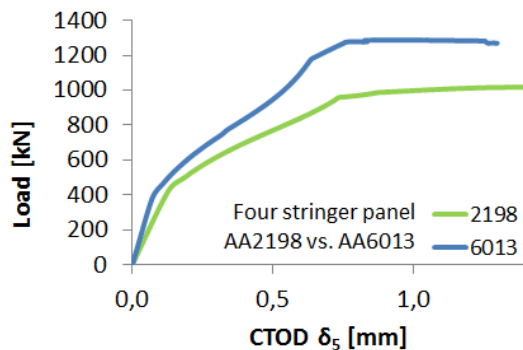


Figure 22: SINTAP analysis, variation 5: AA2198 Vs. AA6013

Because the plastic zone around the crack tip is small compared with the panel size, the high plastic deformability capacity and better CTOD curve will not be enough to make the AA2198 T3 LT comparable to the AA6013 T6 LT. Nevertheless, taking in account the figure 6, it can be expected that a structure composed of solely AA2198 T8 would have better results than the AA6013 T6.

5. Conclusions

The SINTAP procedure proved to be an adequate method to predict the residual strength behavior. Not only from the SINTAP, but, as well from the experimental and numerical work produced, several conclusions are taken.

The fracture resistance of the AA2198 T3 LT is higher than the AA2198 T8 LT. Nevertheless, the

yield stress is higher for the AA2198 T8 and this is the first parameter to take in account when designing a structure.

The SINTAP procedure allowed the prediction of the residual strength for the given structure. Two variations were able to consistently predict the behavior of the panel;

Comparing the AA2198 T3 LT to the AA6013 T6 LT reveals that the last one presents better mechanical fracture performance. An improvement can be expected, in relation to both cases, if the structure is completely made of AA2198 T8 LT due to its high proof strength.

6. Future work

The residual strength test of the four-stringer panel was not enough to make verified observation of the behavior of this type of panel. More residual strength tests would be recommended.

A completely new panel with the skin made of AA2198 T8 would be recommended for test due to its high proof strength.

In order to guarantee a better FEM approximation, a new analysis would be recommended using 3D solid elements in the skin-stringer intersection of the four-stringer panel. It could so happen that the result would not reflect in an improved approximation. The answer can only be known after the analysis.

Following the SINTAP procedure scale of analysis, the Level 2 and Level 5 would be recommended to be followed as well to provide a more complete assessment of the material and structure.

The SINTAP also allows the introduction of secondary stresses such as residual stresses due to LBW. It would be interesting to introduce these effects directly in the SIF distribution.

Acknowledgements

The research work was accomplished at Helmholtz-Zentrum Geesthacht (HZG), at the Institute of Materials Research / Material Mechanics - Department of Joining and Assessment (WMF)

The author would like to thank the help he had at HZG, for all that he was taught and for the given opportunity. Special thanks to Dr. Nikolai Kashaev for his guidance throughout this work and to all the colleagues in the WMF department.

The author is also extremely grateful for Prof. Luis Reis and Prof. Miguel Neves for accompanying him. For all the productive discussions, suggestions, sharing their knowledge and being demanding, they brought motivation and inspiration.

And finally to his family and friends who were missed a lot during this period.

References

- [1] N. Kashae, S. Riekehr, K. Erdmann, A. Carvalho, M. Nurgaliev, N. Alexopoulos, and A. Karanika, "Mechanical fracture behavior of laser beam welded aa2198 butt joints and integral structures," *International Journal of Structural Integrity Conference*, 2014.
- [2] H.-J. Schmidt and B. Schmidt-Brandecker, *Fatigue and Damage Tolerance Course for Metal Structure - Lecture Notes*. AeroStruc, Aeronautical Engineering, 2012.
- [3] H. Vlieger, "The residual strength characteristics of stiffened panels containing fatigue cracks," *Engineering Fracture Mechanics*, vol. 5, pp. 447–477, 1973.
- [4] R. P. Harrison, K. Loosemore, and I. Milne, *Assessment of the integrity of structures containing defects*. CEGB Report R/H/R6, 1976.
- [5] BSI, *PD6493-80. Guidance on Methods for assessing the acceptability of flaws in fusion welded structures*. British Standard Institution, London, 1980.
- [6] K. H. Schwalbe, "The engineering flaw assessment method efam.," *Fatigue and fracture of engineering materials*, vol. 21, pp. 1203–1213, 1998.
- [7] B. Brickstad, M. Bergman, P. Andersson, L. Dahkberg, I. Sattari-Far, and F. Nilson, "Procedure used in sweden for safety assessment of components with cracks.," *International Journal of Pressure Vessels and Piping*, vol. 77, pp. 877–881, 2000.
- [8] C. Faigy, "Rse-m. a general presentation of the french codigied flaw evaluation procedure," *International Journal of Pressure Vessels and Piping*, vol. 77 (2000), pp. 919–927, 2000.
- [9] H. K. et al., "Development of a flaw evaluation handbook of the high pressure institute of japan," *International Journal of Pressure Vessels and Piping*, vol. 77 (2000), pp. 929–936, 2000.
- [10] P. N. Li, Y. Lei, Q. P. Zhong, and X. R. Li, "A chinese structural integrity assessment procedure for pressure vessls containing defects," *International Journal of Pressure Vessels and Piping*, vol. 77 (2000), pp. 945–952, 2000.
- [11] T. L. Anderson and D. A. Osage, "Api 579: A comprehensive fitness-for-service guide," *International Journal of Pressure Vessels and Piping*, vol. 77 (2000), pp. 953–963, 2000.
- [12] K.-H. C. K. H.Schwalbe and J. Heerens, "The engineering treatment model (etm) - a simple method for estimating the driving force under elastic-plastic and plane stress conditions," *Mechanical Engineering Publications*, pp. 1111–1124, 1991.
- [13] E. Seib, *Residual strength analysis of laser beam and friction stir welded aluminium panels for aerospace application*. PhD thesis, GKSS, 2006.
- [14] K.-H. Schwalbe, B. Neale, and J.Heerens, *EFAM GTP 94: The GKSS test procedure for determining the fracture behaviour of materials*. GKSS, 1994.
- [15] K.-H. Schwalbe, D. Hellmann, J. Heerens, J. Knaack, and J. M. Roos, "Measurement of stable crack growth including detection of initiation of growth using the dc potetntial drop and the partial unloading methods," *Elastic-plastic Fracture Test Methods: The User's Experience, ASTM STP 856*, pp. 338–362, 1985.
- [16] T. Kremer and H. Schurmann, "Buckling of tension-loaded thin walled composite plates with cut-outs." *Composites Science and Technology*, 2007.
- [17] P. K. Datta and S. Biswas, "Research advances on tension buckling behaviour of aerospace structures: a review," *International Journal of Aeronautical and Space Sciences*, vol. 12 (1), pp. 1 – 15, 2011.
- [18] H. H. Johnson, "Calibrating the eletric potential method for studying show crack growth," *Material Research Standards*, vol. 5, pp. 442–445, 1965.
- [19] H. Tada, P. C. Paris, and G. R. Irwin, *The stress analysis of cracks handbook - Third Edition*. Professional Engineering Publishing, 2000.
- [20] J. Enz, S. Riekehr, V. Ventzke, and N. Kashae, "Influence of the local chemical composition on the mechanical properties of laser beam welded al-li alloys," *Physics Procedia*, vol. 39 (2012), pp. 51 – 58, 2012.
- [21] M.-V. Uz, M. Kocak, F. Lemaitre, J.-C. Ehrstrom, S. Kempa, and F. Bron, "Improvement of damage tolerance of laser beam welded stiffened panels for airframes via local engineering," *International Journal of Fatigue*, vol. 31 (2009), pp. 916 – 926, 2009.